Computational studies of SiH2+SiH2 recombination reaction dynamics on a global potential surface fitted to ab initio and experimental data

Paras M. Agrawal, Donald L. Thompson, and Lionel M. Raff

Citation: J. Chem. Phys. **88**, 5948 (1988); doi: 10.1063/1.454508
View online: http://dx.doi.org/10.1063/1.454508
View Table of Contents: http://jcp.aip.org/resource/1/JCPSA6/v88/i9
Published by the AIP Publishing LLC.

Computational studies of SiH_2+SiH_2 recombination reaction dynamics on a global potential surface fitted to *ab initio* and experimental data

Paras M. Agrawal,[a] Donald L. Thompson, and Lionel M. Raff
Department of Chemistry, Oklahoma State University, Stillwater, Oklahoma 74078

(Received 14 September 1987; accepted 19 January 1988)

The recombination dynamics for the $SiH_2 + SiH_2 \rightarrow H_2Si = SiH_2$ reaction are studied by quasiclassical trajectory methods using a global potential-energy surface fitted to the available experimental data and the results of various *ab initio* calculations. The potential surface is written as the sum of 18 many-body terms whose functional forms are motivated by chemical and physical considerations. The surface contains 41 parameters which are fitted to calculated geometries, fundamental vibrational frequencies, and energies for $H_2Si = SiH_2$, $H_2Si = SiH$, $H_2Si = Si$, $HSi = Si$, Si_2, H_2, and SiH_2, and to various calculated and/or measured reaction barrier heights and activation energies. In general, the equilibrium bond lengths and angles given by the global surface are in agreement with *ab initio* results to within 0.03 Å and 0.5°, respectively. The calculated exothermicities for various reactions involving silicon and hydrogen atoms are in excellent agreement with previous MP4 calculations and with experimental data. The average absolute error is 1.90 kcal/mol. The average absolute deviation of the predicted fundamental vibrational frequencies for $H_2Si = SiH_2$, $H_2Si = SiH$, $H_2Si = Si$, and SiH_2 from the results reported by Ho *et al.* is 52.9 cm^{-1}. The calculated barrier height for molecular hydrogen elimination from SiH_2 is 34.27 kcal/mol with a backreaction barrier of 0.63 kcal/mol. The barrier for 1,2 elimination of H_2 from $H_2Si = SiH_2$ is 115.3 kcal/mol with a backreaction barrier of 30.7 kcal/mol. The formation cross sections for $H_2Si = SiH_2$ decrease with both relative translational energy and internal SiH_2 energy with translational energy being the more effective in reducing the cross sections. Thermally averaged formation cross sections vary from 66.3 $Å^2$ at 300 K to 28.7 $Å^2$ at 1500 K. The corresponding thermal rate coefficients lie in the range $2\text{–}4\times10^{14}$ cm^3/mol s over this temperature range and exhibit a maximum at an intermediate temperature. The trajectory details indicate that the reaction exothermicity is primarily partitioned into the Si–Si stretch and the H–Si–H bending modes upon formation of Si_2H_4. Energy transfer from the Si–Si stretch to the Si–H stretching modes is a relatively slow process occurring on a time scale of 10^{-12} s, which is about three to four times that previously computed for other polyatomic systems. Transfer from the Si–Si stretch to the H–Si–H bending modes is a faster process.

I. INTRODUCTION

The modeling studies reported by Coltrin *et al.*[1] suggest that the Si_2 dimer makes a significant contribution (up to 50%) to the total silicon chemical vapor deposition (CVD) rate provided the temperature is in excess of 1150 K and the carrier gas is helium. Ho and Breiland[2] have also observed Si_2 in silicon CVD using laser excited fluorescence. The elementary steps leading to the formation of Si_2 are unknown. The mechanism could involve simple termolecular recombination

$$Si + Si + M \longrightarrow Si_2 + M, \qquad (1)$$

where M represents any third body. We have previously calculated the expected rates for reaction (1) when M is an argon atom.[3] The results give rate coefficients of 6.3×10^{13}, 7.0×10^{13}, and 9.5×10^{13} cm^6/mol s at temperatures of 200, 250, and 300 K, respectively. The activation energy for the recombination is 0.47 kcal/mol.[4] The low concentration of silicon atoms present in typical CVD experiments, however, argues against reaction (1) being the major pathway leading to silicon dimer formation.

A more plausible mechanism involves polymerization–decomposition reactions. Coltrin *et al.*[1] have suggested that the sequence

$$SiH_4 + SiH_2 \longrightarrow Si_2H_6, \qquad (2A)$$

$$Si_2H_6 \longrightarrow Si_2H_4 + H_2, \qquad (2B)$$

$$Si_2H_4 \longrightarrow Si_2H_2 + H_2, \qquad (2C)$$

$$Si_2H_2 \longrightarrow Si_2 + H_2 \qquad (2D)$$

constitutes the major pathway for dimer formation. The high concentration of silane and the fact that SiH_2 is the primary dissociation product of silane unimolecular dissociation[5] argue in favor of this mechanism. Unfortunately, the rates of the individual steps in process (2) are unknown. Consequently, a quantitative comparison of the overall Si_2 formation rates via paths (1) and (2) is not possible.

The complexity of the Si_2H_6 system makes quantitative calculations of the formation/decomposition rates particularly difficult. As a first approach to such a study, we have therefore chosen to investigate the analogous reactions in-

[a] On leave from Vikram University, Ujjain, MP, India.

 0021-9606/88/095948-15$02.10

volving the recombination and subsequent decomposition of two silylene molecules:

$$SiH_2 + SiH_2 \longrightarrow SiH_2 = SiH_2, \quad (3A)$$

$$SiH_2 = SiH_2 \longrightarrow SiH_2 + SiH_2, \quad (3B)$$

$$SiH_2 = SiH_2 \longrightarrow SiH_2 = SiH + H, \quad (3C)$$

$$SiH_2 = SiH \longrightarrow SiH_2 = Si + H, \quad (3D)$$

$$SiH_2 = SiH_2 \longrightarrow SiH_2 = Si + H_2, \quad (3E)$$

$$SiH_2 = Si \longrightarrow SiH = Si + H, \quad (3F)$$

$$SiH = Si \longrightarrow Si_2 + H, \quad (3G)$$

$$SiH_2 = Si \longrightarrow Si_2 + H_2, \quad (3H)$$

$$SiH_2 = SiH \longrightarrow SiH = SiH + H, \quad (3I)$$

$$SiH_2 = SiH_2 \longrightarrow SiH = SiH + H_2, \quad (3J)$$

$$SiH = SiH \longrightarrow SiH = Si + H, \quad (3K)$$

$$SiH = SiH \longrightarrow Si_2 + H_2. \quad (3L)$$

Reactions (3A) and (3B) represent the reversible formation/decomposition steps for disilene. Reactions (3C)–(3I) and (3K) are the two- and three-center elimination processes leading to atomic and molecular hydrogen. Reactions (3J) and (3L) are four-center, 1,2-hydrogen elimination reactions leading to $(SiH)_2$ and Si_2, respectively. Although complex, this six-body system is significantly easier to handle than the corresponding set of reactions for the eight-atom Si_2H_6 system. Furthermore, reactions (3C)–(3L) are the processes that are involved in steps (2C) and (2D) in the disilane decomposition. The present studies will therefore yield part of the information required to quantitatively assess the importance of the Eq. (2) pathway.

The most crucial part of any theoretical study of reaction dynamics is the formulation of a sufficiently accurate potential-energy hypersurface. In the present case, the size of the system makes this a particularly difficult step. Fortunately, several groups have reported the results of extensive *ab initio* calculations of a variety of topographical features of the Si_2H_4 surface. In addition, some experimental measurements of activation energies, bond energies, and fundamental vibrational frequencies are also available. In order to utilize this information in a dynamics calculation, a global potential surface must be constructed. Ideally, this surface would incorporate all of the existing data accurately in such a manner that all important reaction channels are represented.

In Sec. II, we report the results of an effort to develop a global potential for the Si_2H_4 system. With such a surface, the SiH_2 recombination cross sections and thermal rate coefficients can be computed using standard trajectory techniques. The microcanonical and thermal dissociation rate coefficients for Si_2H_4 can be calculated using either trajectories, transition-state theory, variational transition-state theory,[6] or variational phase-space theory.[7] The nature and rates of intramolecular energy transfer in Si_2H_4, which is important in the determination of the lifetimes of Si_2H_4 formed via reaction (3A), can likewise be examined. Section III reports formation cross sections as a function of relative translational energy and initial SiH_2 vibrational and rotational energy for reaction (3A). Thermal rate coefficients for this reaction are also determined as a function of temperature. Subsequent papers will deal with the dissociation dynamics of Si_2H_4 and with intramolecular energy transfer in this molecule.

II. Si_2H_4 POTENTIAL-ENERGY SURFACE

A. Functional form

Many of the stationary points on the Si_2H_4 potential surface have been well characterized by previously reported *ab initio* studies. In addition, the saddle-point energies for some of the transition states have also been computed. Ho *et al.*[8,9] have carried out calculations at the Hartree–Fock level using 6-31G* basis sets to determine the equilibrium geometries of SiH_n ($n \leqslant 4$) and Si_2H_n $n = 0$–6). Bond enthalpies and transition-state enthalpies were computed using fourth-order Möller–Plesset perturbation theory[10] with 6-31G** basis sets. In addition, an empirical correction procedure was utilized to account for systematic errors in the *ab initio* total energy calculations for Si–H and Si–Si bonds that arose from the truncated wave functions and incomplete basis sets. Fundamental vibrational frequencies for each molecule investigated are also reported.

Gordon *et al.*[11] have also reported *ab initio* studies at the MP4/MC-311G** level at geometries calculated with SCF wave functions and 3-21G, 6-31G, or 6-31G** basis sets for the species involved in the pyrolysis of disilane. Equilibrium geometries for SiH_n ($n = 1$–3), $SiH_2 = SiH_2$, SiH_3–SiH, and Si_2H_6 are reported as well as fundamental vibration frequencies for disilane, disilene, SiH_2, SiH_3, SiH_4, and SiH_3–SiH. A variety of transition-state structures for the decomposition of silane have been investigated.

Poirier and Goddard[12] and Krogh-Jespersen[13] have reported *ab initio* studies of disilene. Poirier and Goddard carried out CI calculations with a 3-21G basis set while Krogh-Jespersen used MP3/6-31G** calculations at MP2/6-31G* geometries. Both of these studies showed disilene to be more stable than its isomer, silyl silylene.

Configuration interaction studies of the Si_2 dimer have been reported by Peyerimhoff and Buenker.[14] Their results include potential curves for the Si_2 ground state and many of the excited electronic states. At large Si–Si separations, the ground state is $^1\Sigma_g^-$. At smaller internuclear distances, there is a curve crossing and the $^3\Pi_u$ potential becomes the lowest-energy state.

In addition to these theoretical studies, several experimental studies have been reported that yield useful information related to the topography of the Si_2H_4 potential surface. Berkowitz *et al.*[15] have obtained Si–H bond dissociation energies for SiH_4, SiH_3, SiH_2, and SiH from the results of photoionization mass spectrometric studies of SiH_n ($n = 1$–4). X-ray measurements of the structure of disilene have been reported by West *et al.*[16] and by Fink *et al.*[17] Jasinski[18] has obtained an upper limit for the activation energy for the insertion reaction of D_2 into SiH_2 using laser resonance absorption flash kinetic spectroscopy. Similiar results have also been reported by Inoue and Suzuki[19] using laser induced fluorescence. Huber and Herzberg[20] have reported a dissociation energy for the Si_2 dimer.

As a result of these studies, a great deal of information concerning the Si_2H_4 potential-energy surface is available. In order to utilize these results in dynamics calculations, however, it is necessary to develop an analytical global potential function that adequately fits as much of this data as possible. Our approach is to adopt physically motivated functional forms for the stretching and bending interactions of the system. The parameters of these functions are then adjusted to fit the available experimental and *ab initio* data.

It is most convenient to express such a global potential in terms of the interatomic distances and bond angles. For this purpose, we adopt the atom numbering and distance notation illustrated in Fig. 1. R_1 is the Si–Si distance. R_i ($i = 2,3,...,9$) and R_j ($j = 10,11,...,15$) are the Si–H and H–H distances, respectively. We define the H–Si–H angles to be θ_1 and θ_2 for silicon atoms 1 and 2, respectively. The Si–Si–H angles are denoted by θ_i ($i = 3$–6) as shown in Fig. 1. The dihedral angle between the two SiH_2 groups is denoted by Φ.

Formally, we choose to write the Si_2H_4 potential in the form

$$V = V_{SiH_2}(R_2,R_3,R_{10}) + V_{SiH_2}(R_4,R_5,R_{15}) + V_{Si_2}(R_1) + \sum_{i=3}^{6} 0.5k_a[\theta_i - \theta_i^0]^2 + \sum_{j=11}^{14} V_{HH}(R_j) + V_T(\Phi) . \quad (1)$$

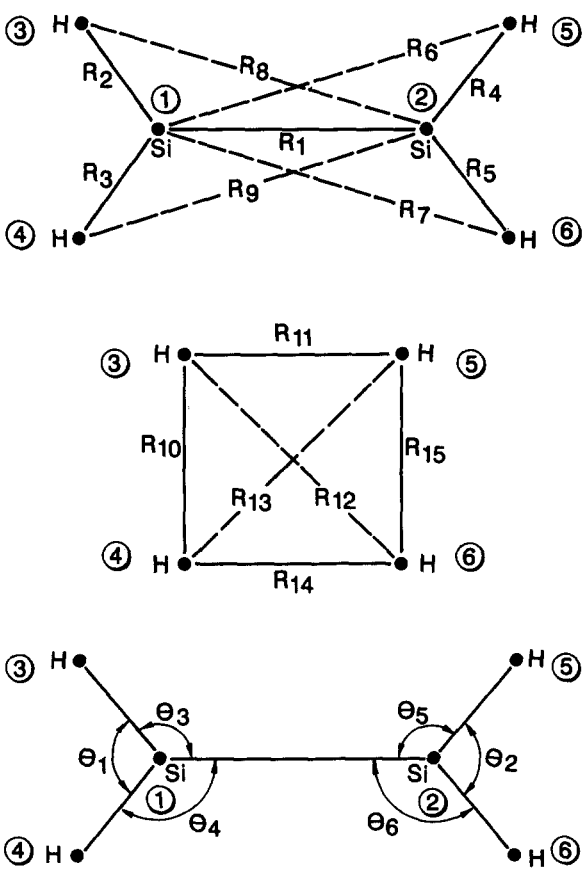

FIG. 1. Definition of interatomic distance and angle notation. The atom number designations are circled.

Each of the terms in Eq. (1) is functionally dependent upon several interatomic distances. The notation used for the arguments of the terms therefore serves only to identify the group of atoms, bond, or angle whose interaction is described by the term. The first two terms in Eq. (1) describe the force fields for the two SiH_2 groups. These terms are given by

$$V_{SiH_2}(R_i,R_j,R_k) = V_{SiH}(R_i) + V_{SiH}(R_j) + V_H(R_k) + 0.5k_b[\theta - \theta^0]^2 , \quad (2)$$

where θ is the angle formed by the vectors $\mathbf{R}_i$ and $\mathbf{R}_j$. As in Eq. (1), the arguments serve only to identify the bond or angle involved in the interaction. All terms are dependent upon several interatomic distances. Thus, the first two terms in Eq. (2) describe the Si–H stretching interactions. The third and fourth terms give the H–H and bending interactions, respectively.

The choice of functional forms for the above terms is dictated by several considerations. First, we wish the form to be physically reasonable. Thus, we prefer a Morse-type function to represent a stretching interaction rather than an expansion in terms of arbitrarily chosen functions. Second, we require that the asymptotic limits of the functions properly describe the molecules formed, and third, we require the functions to have sufficient flexibility to allow them to be fitted to the existing *ab initio* and experimental data. For the Si–H stretching interactions, we choose a Morse-type term,

$$V_{SiH}(R_i) = D_{SiH}\{\exp[-2\alpha_{SiH}(R_i - R_i^0)] - 2\exp[-\alpha_{SiH}(R_i - R_i^0)]\}A_3 . \quad (3)$$

The "parameters" of this function, D_{SiH}, α_{SiH}, and R_i^0, are actually functions of the interatomic distances

$$D_{SiH} = [D_2 + (D_1 - D_2)S_1(R_1)] - [\Delta_2 + (\Delta_1 - \Delta_2)S_1(R_1)]S_2(R_i,R_j), \quad (4)$$

where the switching functions, $S_1(R_1)$ and $S_2(R_i,R_j)$, are given by

$$S_1(R_1) = B(1,0)\tanh[C_1(R_1 - R_1^0)] , \quad (5)$$

where $B(1,0)$ is unity if the argument of the hyperbolic function is positive and zero otherwise, and

$$S_2(R_i,R_j) = B(1,0)\tanh\{C_2(R_i + R_j - 2R_2^0)\} . \quad (6)$$

α_{SiH} and R_i^0 are similarly defined:

$$\alpha_{SiH} = \alpha_2 + (\alpha_1 - \alpha_2)S_1(R_1) , \quad (7)$$

$$R_i^0 = C_3 + (C_4 - C_3)S_1(R_1) . \quad (8)$$

The $S_1(R_1)$ function produces a monotonic change in the Si–H bond energies, curvatures, and equilibrium distances from those characteristic of SiH_2 to those appropriate for $H_2Si{=}SiH_2$ as $R_1 \to R_1^0$. $S_2(R_i,R_j)$ performs a similar function for the SiH_2 moiety. As either R_i or R_j increases, this function alters the Si–H bond energy from the measured value for SiH_2 to that for SiH. The A_3 function causes the Si–H bond to attenuate as an H–H bond forms. Its form is

$$A_3 = \prod_j \{1.0 - \exp[-C_9(R_j - R_H^0)^2]\} , \quad (9)$$

where the index j runs over the three H–H distances asso-

ciated with the hydrogen atom forming the Si–H bond.

The H–H stretching term is

$$V_H(R_k) = D_H\{\exp[-2\alpha_H(R_k - R_H^0)] - 2\exp[-\alpha_H(R_k - R_H^0)]\}A_1(R_i,R_j), \quad (10)$$

with

$$A_1(R_i,R_j) = 0.5\{2.0 - \exp[-C_5(R_i - R_2^0)^2] - \exp[-C_5(R_j - R_2^0)^2]\}. \quad (11)$$

The $A_1(R_i,R_j)$ function attenuates the H–H bonding as the two Si–H bonds form.

The force "constant," k_b, and the equilibrium angle, θ^0, in the H–Si–H bending term are defined to be

$$k_b = [k_2 + (k_1 - k_2)S_1(R_1)] \times \exp\{-C_6[(R_i - R_2^0)^2 + (R_j - R_2^0)^2]\} \quad (12)$$

and

$$\theta^0 = C_7 + (C_8 - C_7)S_1(R_1). \quad (13)$$

Here, the $S_1(R_1)$ factor serves to vary the effective bending force constant as reaction (3A) occurs. The exponential factor attenuates the bending interaction as either bond is broken. Previous studies have shown such attenuation factors to be nearly Gaussian in form.[21]

The third term in Eq. (1) describes the Si–Si interaction. Its form is analogous to that for the Si–H terms described by Eqs. (3)–(7):

$$V_{Si_2}(R_1) = D_s\{\exp[-2\alpha_s(R_1 - R_s^0)] - 2\exp[-\alpha_s(R_1 - R_s^0)]\}, \quad (14)$$

with

$$D_s = D_4 + (D_3 - D_4) \times \tanh[C_{10}(R_2 + R_3 + R_4 + R_5 - 4.2C_3)]B(1,0), \quad (15)$$

$$\alpha_s = \alpha_4 + (\alpha_3 - \alpha_4) \times \tanh[C_{11}(R_2 + R_3 + R_4 + R_5 - 4.2C_3)]B(1,0), \quad (16)$$

and

$$R_s^0 = C_{12} + (C_{13} - C_{12}) \times \tanh[C_{14}(R_2 + R_3 + R_4 + R_5 - 4.2C_3)]B(1,0) - C_{15}\{\tanh[C_{16}(R_2 - C_3)] \times \tanh[C_{16}(R_3 - C_3)]B(1,0) + \tanh[C_{16}(R_4 - C_3)] \times \tanh[C_{16}(R_5 - C_3)]B(1,0)\}. \quad (17)$$

The hyperbolic functions in Eqs. (15) and (16) vary the Si–Si bond energy and curvature appropriately as reaction (3C) occurs. In Eq. (17), the first hyperbolic function performs the same function for the equilibrium distance as it does for the bond energy and curvature as reaction (3C) occurs. The last four hyperbolic functions vary the equilibrium distance as reaction (3D) takes place.

The force constant and equilibrium angles in the Si–Si–H bending terms in Eq. (1) are defined in a manner analogous to that for the H–Si–H bending interactions:

$$k_a = k_a^0 \exp\{-C_{17}[(R_u - R_u^0)^2 + (R_v - R_v^0)^2]\}, \quad (18)$$

where R_u and R_v are the interparticle distances forming the angle θ_i and R_u^0 and R_v^0 are the equilibrium distances for interparticle distances R_u and R_v, respectively,

$$\theta_i^0 = C_{18} + (C_{19} - C_{18})\{\tanh[C_{16}(R_2 - C_3)] \times \tanh[C_{16}(R_3 - C_3)]B(1,0) + \tanh[C_{16}(R_4 - C_3)] \times \tanh[C_{16}(R_5 - C_3)]B(1,0)\}. \quad (19)$$

The four-center H–H interaction terms are

$$V_{HH}(R_i) = D_H \exp[-2\alpha_H(R_i - R_H^0)] - 2\exp[-\alpha_H(R_i - R_H^0)] \times A_2(R_u,R_v)A_4(R_{10},R_{11},R_{12},R_{13},R_{14},R_{15}), \quad (20)$$

where

$$A_2(R_u,R_v) = 0.5\{2.0 - \exp[-C_{22}(R_u - C_3)^2] - \exp[-C_{22}(R_v - C_3)^2]\} \quad (21)$$

and

$$A_4(R_{10},R_{11},R_{12},R_{13},R_{14},R_{15}) = \prod_{\substack{j=10 \\ j\neq i, j\neq k}}^{15} B(1,0)\tanh[\beta(R_j - R_H^0)]. \quad (22)$$

In Eq. (21), R_u and R_v are the Si–H bonds being broken to form the H_2 molecule. In Eq. (22), k represents the interatomic distance between the two hydrogen atoms not involved in the $V_{HH}(R_i)$ term. The $A_2(R_u,R_v)$ function causes the attenuation of the H–H bond as the two Si–H bonds form. The A_4 function serves to prevent the formation of multiple hydrogen bonds which would lead to species such as H_3 or H_4.

The torsional term in Eq. (1) is

$$V_T(\Phi) = k_\phi\Phi^2\{1.0 - \tanh[C_{21}(R_2 - R_2^0)]B(1,0)\} \times \{1.0 - \tanh[C_{21}(R_3 - R_2^0)]B(1,0)\} \times \{1.0 - \tanh[C_{21}(R_4 - R_2^0)]B(1,0)\} \times \{1.0 - \tanh[C_{21}(R_5 - R_2^0)]B(1,0)\} \times \{1.0 - \tanh[C_{21}(R_1 - R_1^0)]B(1,0)\}. \quad (23)$$

The hyperbolic functions attenuate the torsional interaction as any Si–H bond breaks or upon rupture of the Si–Si bond.

Equation (1) contains 41 parameters. D_1, D_2, Δ_1, and Δ_2 are adjusted to fit the *ab initio* and experimental results for the Si–H bond enthalpy in SiH, SiH_2, $H_2Si=SiH_2$, and

$H_2Si = SiH$. D_H is fitted to the known H_2 well depth. D_3 and D_4 are determined from the calculated Si–Si bond enthalpies for $H_2Si = SiH_2$ and $H_2Si = SiH$. R_1^0 is adjusted to be slightly larger than the calculated Si–Si equilibrium bond lengths. R_2^0, C_3, and C_4 are obtained from the calculated equilibrium Si–H bond lengths in Si–H and SiH_2. C_{12}, C_{13}, and C_{15} are adjusted to the calculated equilibrium Si–Si bond lengths for $H_2Si = SiH_2$, $H_2Si = SiH$, and $H_2Si = Si$. α_1 and α_2 are used to adjust the symmetric and asymmetric fundamental stretching frequencies for SiH_2 to the *ab initio* and experimental results. α_H and R_H^0 are obtained from the H_2 fundamental vibrational frequency and equilibrium bond length, respectively. α_3, α_4, k_1, k_2, k_a^0, k_ϕ, C_6, and C_{17} are fitted to the calculated fundamental vibrational frequencies for $H_2Si = SiH_2$. C_7, C_8, C_{18}, and C_{19} are adjusted to yield the correct equilibrium H–Si–H and Si–Si–H angles in SiH_2, $H_2Si = SiH_2$, and $H_2Si = Si$. C_2, C_5, and C_9 are used to adjust the barrier height for the backreaction $H_2 + Si \rightarrow SiH_2$ so that it is in accord with the experimental data reported by Jasinski[18] and by Inoue and Suzuki.[19] The barrier height for 1,2 elimination of H_2 from $H_2Si = SiH_2$ is adjusted to be in accord with the *ab initio* calculations reported by Ho *et al.*[8,9] using C_{22}. β is adjusted so that the Si_2H_4 potential predicts the correct barrier height for the hydrogen exchange reaction $H + H_2 \rightarrow H_2 + H$. The remaining parameters, C_1, C_{10}, C_{11}, C_{14}, C_{16}, and C_{21}, control the rate at which the limiting asymptotic forms are approached. Since there is neither experimental data nor *ab initio* results currently available that gives any information related to these topographical features of the Si_2H_4 surface, these parameters have been assigned the arbitrary value of 1.0 except for C_1 which is taken to be 0.5. Should additional *ab initio* results become available, these parameters are available for appropriate adjustment of the surface. Table I gives the values for all parameters.

TABLE I. Potential-surface parameters.

Parameter	Value
D_1 (eV)	3.117 95
D_2 (eV)	3.117 95
Δ_1 (eV)	0.164 80
Δ_2 (eV)	0.919 338
D_3 (eV)	3.148 30
D_4 (eV)	3.482 20
D_H (eV)	4.746 60
R_1^0 (Å)	2.500 00
R_2^0 (Å)	1.512 00
C_3 (Å)	1.468 00
C_4 (Å)	1.512 00
R_H^0 (Å)	0.741 90
C_{12} (Å)	2.132 00
C_{13} (Å)	2.314 00
C_{15} (Å)	0.127 00
C_1 (1/Å)	0.500 00
C_2 (1/Å)	2.000 00
α_1 (1/Å)	1.866 00
α_2 (1/Å)	1.925 00
α_H (1/Å)	1.898 165
α_3 (1/Å)	1.830 00
α_4 (1/Å)	1.566 00
C_{10} (1/Å)	1.000 00
C_{11} (1/Å)	1.000 00
C_{14} (1/Å)	1.000 00
C_{16} (1/Å)	1.000 00
C_{21} (1/Å)	1.000 00
β (1/Å)	1.745 00
C_7 (rad)	1.971 40
C_8 (rad)	1.610 90
C_{18} (rad)	2.075 00
C_{19} (rad)	2.154 00
k_1 (eV/rad^2)	4.154 00
k_2 (eV/rad^2)	2.758 00
k_ϕ (eV/rad^2)	0.135 00
k_a^0 (eV/rad^2)	1.900 00
C_5 (Å^{-2})	15.000 00
C_6 (Å^{-2})	1.500 00
C_9 (Å^{-2})	15.000 00
C_{17} (Å^{-2})	0.450 00
C_{22} (Å^{-2})	6.000 00

B. Properties of the surface

1. Equilibrium structures and heats of reaction

The equilibrium structures and associated energies have been determined by using trajectories in which all momenta are set to zero each time the kinetic energy attains a maximum. This procedure is repeated until the structure converges to a local minimum. By sampling different initial configurations, the equilibrium structures can be obtained. The results for $H_2Si = SiH_2$, $H_2Si = SiH$, $H_2Si = Si$, $HSi = SiH$, SiH_2, and Si_2 are shown in Fig. 2. Table II compares the structures with *ab initio* calculations reported by Ho *et al.*,[8,9] Gordon *et al.*,[11] and Binkley.[22]

The results for $H_2Si = SiH_2$ are in excellent accord with the MP4 calculations reported by Ho *et al.*[9] The predicted Si–Si separations are in exact agreement and the Si–H distance is low by 0.014 Å. The MP4 calculations reported by Gordon[11] use a slightly different basis set. The differences between the equilibrium bond lengths predicted by the global surface and these results are on the order of 0.02–0.03 Å. The equilibrium bond angles given by Eq. (1) are in very good agreement with the values reported by Gordon *et al.*[11] The maximum deviation is less than 0.5°. Ho *et al.*[9] did not report equilibrium bond angles.

Equation (1) predicts an equilibrium structure for $H_2Si = SiH$ which is also in good accord with *ab initio* MP4 results.[9] The predicted Si–Si separations are identical. The global surface yields Si–H distances about 0.02–0.03 Å less than the MP4 computations. A similar level of accuracy is achieved for the Si–Si and Si–H bond lengths for $H_2Si = Si$.[9] The H–Si–Si angle is in excellent accord with the value obtained by Binkley[22] using HF/6-31G** methods. The H–Si–H angle, however, differs from Binkley's result by + 4.1°.

The results for *trans*-bent disilyne, $HSi = SiH$, are not in good agreement with the HF/6-31G** calculations.[22] The Si–H equilibrium distance agrees well, but the Si–Si distance differs by 0.23 Å. The H–Si–Si angle is also smaller by 8.6°. To some extent, this discrepancy may be due to the fact that the *ab initio* calculations were done at the SCF level without correction for correlation energy. However, for the greater part, this difference reflects lack of flexibility in the global surface. The parameters of the surface were not adjusted to

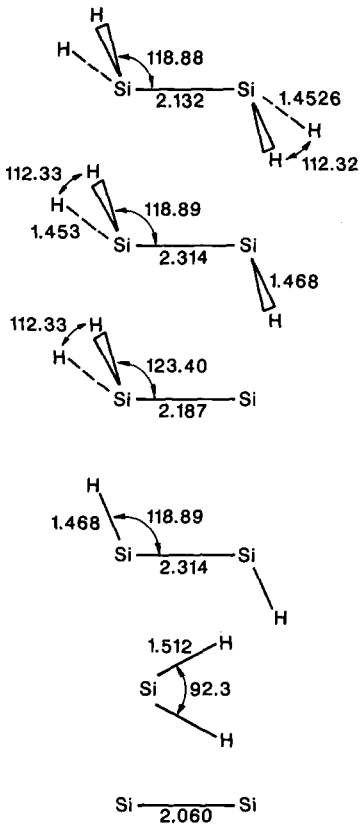

FIG. 2. Equilibrium structures predicted by Eq. (1) for several Si_nH_m molecules. Angles are in degrees and distances in Å.

the HSi = SiH results. Consequently, differences of the magnitude cited are not surprising.

The equilibrium geometry predicted by Eq. (1) for SiH_2 is in nearly exact agreement with results reported by Ho *et al.*[8] and by Gordon *et al.*[11]

The heats of reaction for reactions (3A)–(3L) predicted by Eq. (1) are summarized in Table III where they are compared with the *ab initio* results reported by Ho *et al.*[8,9] and by Peyerimhoff and Buenker[13] and with the experimental data obtained by Berkowitz *et al.*[14] As can be seen, the results are uniformly excellent. The accuracy for the calculated endothermicity for reaction (3J), the four-center 1,2-hydrogen elimination to form *trans*-bent disilyne, is more difficult to assess. Ho *et al.*[9] estimate this endothermicity to be greater than 73 kcal/mol. If this estimate is correct, then Eq. (1) predicts a result 11.6 kcal/mol too large. The average absolute error for all results is 1.90 kcal/mol and almost all of this error is due to reaction (3J).

2. Fundamental vibration frequencies

The fundamental vibration frequencies predicted by Eq. (1) for $H_2Si = SiH_2$, $H_2Si = SiH$, $H_2Si = Si$, and SiH_2 have been determined by computation of the spectral intensities for these molecules. Since the global surface contains only nine parameters which are available for adjustment of the vibrational frequencies, it is not possible to obtain an exact fit to the 30 frequencies exhibited by these four molecules. Nevertheless, the fact that the functional forms contained in Eq. (1) are physically reasonable permits a fair-to-good fit to be obtained. The average absolute deviation of the predicted frequencies from those reported by Ho *et al.*[8,9] is 52.9 cm^{-1}. Only in a few cases are the differences larger than 100 cm^{-1}.

The spectral intensity is calculated directly from the Fourier transforms, $C_a(m\Delta\nu)$, of a set of momentum components, bond angles, or bond lengths:

TABLE II. Equilibrium structures. Distances are given in angstroms. Angles are given in degrees.

Molecule	Variable	Present cal. [Eq. (1)]	*Ab initio*	
$H_2Si = SiH_2$	R(Si–Si)	2.132	2.132[a]	2.169[b]
	R(Si–H)	1.4526	1.468[a]	1.475[b]
	∠H–Si–H	112.32		112.8[b]
	∠H–Si–Si	118.88		118.9[b]
$H_2Si = SiH$	R(Si–Si)	2.314	2.314[a]	
	R(Si–H)	1.453, 1.453, 1.468	1.480, 1.478, 1.500[a]	
	∠H–Si–H	112.33	...	
	∠H–Si–Si	118.89	...	
$H_2Si = Si$	R(Si–Si)	2.187	2.187[a]	2.310[c]
	R(Si–H)	1.453	1.474[a]	1.479[c]
	∠H–Si–H	112.33		108.2[c]
	∠H–Si–Si	123.40		123.4[c]
HSi = SiH	R(Si–Si)	2.314		2.083[c]
	R(Si–H)	1.468		1.478[c]
	∠H–Si–Si	118.89		127.5[c]
SiH_2	R(Si–H)	1.512	1.509[a]	1.512[b]
	H–Si–H	92.3		92.3[b]
Si_2	R(Si–Si)	2.060	2.23[d]	

[a] References 8 and 9.
[b] Reference 11.
[c] Reference 22.
[d] Reference 14.

TABLE III. Heats of reaction. Units are kcal/mol.

Reaction	Present cal.	*Ab initio* or Expt.
$SiH_2 \rightarrow SiH + H$	75.62	75.7[a] 75.6[b]
$SiH \rightarrow Si + H$	68.10	68.1[a] 68.7[b]
$H_2Si = SiH_2 \rightarrow SiH_2 + SiH_2$	80.45	80.3[a]
$H_2Si = SiH_2 \rightarrow H_2Si = SiH + H$	100.8	100.8[a]
$H_2Si = SiH \rightarrow H_2Si = Si + H$	50.7	50.7[a]
$H_2Si = Si \rightarrow H_2Si + Si$	72.7	72.0[a]
$H_2Si = SiH_2 \rightarrow HSi = SiH + H_2$	84.59	>73[a]
$Si_2 \rightarrow Si + Si$	72.60	69.9[c]

[a] References 8 and 9.
[b] Reference 15.
[c] Reference 14.

$$C_a(m\Delta\nu) = N^{-1} \sum_{n=0}^{N} \exp[2\pi i n m/N] S_a(n\Delta t) . \quad (24)$$

In Eq. (24), $S_a(n\Delta t)$ represents either a momentum component, bond angle, or bond length at time $t = n\Delta t$ ($n = 0,1,2,...,N$) in a trajectory of duration τ. The spectral intensity $g(m\Delta\nu)$ is defined to be the sum of the normalized power spectra for each $S_a(n\Delta t)$:

$$g(m\Delta\nu) = \sum_a \left[|C_a(m\Delta\nu)|^2 \Big/ \sum_m |C_a(m\Delta\nu)|^2 \right] . \quad (25)$$

Figure 3 shows the calculated spectral intensity for Si_2H_4 where the $S_a(n\Delta t)$ are the four Si–H bond distances, the Si–Si distance, the four Si–Si–H angles, the two H–Si–H angles, and the dihedral angle. The four Si–H stretching frequencies appear as two unresolved peaks at 2207 and 2352 cm^{-1}. The H–Si–H bend appears as an intense band at 960 cm^{-1}. A small shoulder on this peak around 880 cm^{-1} is evident. We assign this to the SiH_2 rock. The Si–Si stretching mode and H–Si–Si bend appear as two unresolved bands around 550 cm^{-1}. If we use the peak maxima as the band frequencies, the two modes fall at 544 and 560 cm^{-1} for the bend and Si–Si stretch, respectively. Low-frequency modes at 192, 288, 368, and 448 cm^{-1} are also evident. The 368 cm^{-1} band is assigned to the SiH_2 twist, the others to H–Si–Si bending modes.

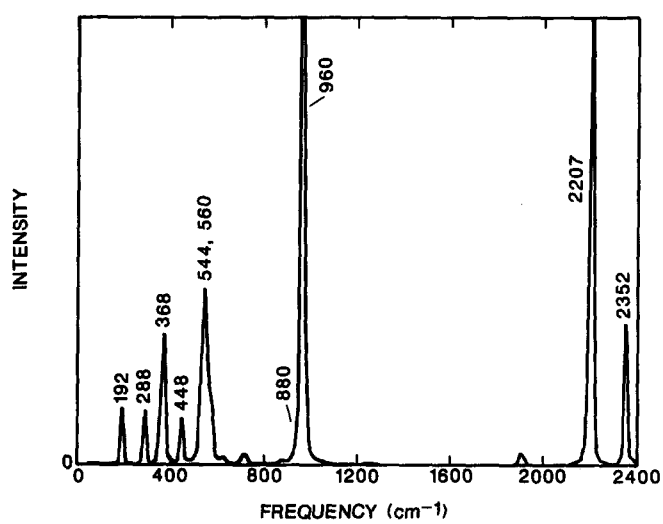

FIG. 3. Vibrational power spectrum for Si_2H_4.

In the above calculations, the total internal energy of Si_2H_4 is 0.0957 eV which is 11.6% of the total Si_2H_4 zero-point energy predicted by the global surface. 94% of this energy is initially equipartitioned among the four hydrogen atoms with the remaining 6% equally divided between the two silicon atoms. Under these conditions, the fundamental frequencies obtained from Eq. (25) will approach those that would result from a harmonic approximation. Similar calculations for $H_2Si = SiH$ and $H_2Si = Si$ have been carried out at total internal energies of 0.0757 and 0.0557 eV, respectively.

Table IV compares the results obtained for $H_2Si = SiH_2$, $H_2Si = SiH$, $H_2Si = Si$, and SiH_2 with the *ab initio* harmonic calculations reported by Ho *et al.*[8,9]

3. Barrier heights and reaction profiles

We have determined approximate reaction profiles and barrier heights for reactions (3B) and (3J) on our global potential-energy surface. In the latter case, it is assumed that the dissociation occurs via a concerted, planar elimination pathway. We have also obtained potential-energy contour maps, reaction profiles, and barrier heights for the elimination of molecular hydrogen from SiH_2,

$$SiH_2 \rightarrow Si + H_2. \quad (4)$$

Figure 4 shows the calculated reaction profile for reaction (3B) in which the Si–H distances are held at their equilibrium value in disilene throughout the dissociation. The energy zero is the separated atoms. As can be seen, there is a monotonic rise in the potential as $2SiH_2$ forms. Consequently, the global surface predicts that the formation reaction (3A) occurs on a purely attractive surface with no barrier. We may therefore expect the calculated formation cross sections to increase as the SiH_2–SiH_2 relative translational energy decreases.[23]

The calculated reaction profile for reaction (4) is shown in Fig. 5. This profile is obtained by investigation of symmetric C_{2v} dissociation pathways in the following manner. The two hydrogen atoms are each displaced by a small amount δ along lines that make an angle α with the symmetry axis of

TABLE IV. Comparison of fundamental vibrational frequencies obtained from the calculated spectral intensities using the global surface, Eq. (1), to the results reported by Ho *et al.* in Refs. 8 and 9. Frequencies are given in cm^{-1}.

Normal mode symmetry	Global surface $H_2Si = SiH_2$	Ho *et al.*
A_g	192	126.34
A_u	368	355.14
A_u	288	533.07
B_u	448	549.31
A_g	560	575.73
B_g	544	593.17
B_u	880	872.21
A_g	960	941.80
B_u	2207	2193.75
A_g	2207	2203.31
B_g	2352	2210.24
A_u	2352	2218.66
	$H_2Si = SiH$	
A	96	322.19
A	160	382.96
A	272	414.44
A	528	439.30
A	640	652.77
A	960	929.02
A	2112	2042.04
A	2112	2138.34
A	2240	2152.29
	$H_2Si = Si$	
B_2	144	323.50
B_1	288	386.49
A_1	624	525.79
A_1	976	895.39
A_1	2208	2163.17
B_2	2240	2179.82
	SiH_2	
A_1	1008	999.83
A_1	2064	2011.69
B_2	2000	2001.72

the molecule. The system potential is computed after each displacement step. At the point at which the two hydrogen atoms are separated by R_H^0, the displacement direction is altered to be parallel to the molecular symmetry axis. This procedure is repeated using different values of the angle α until the reaction profile with the minimum barrier is attained. On the global surface, this occurs for $\alpha = 21°$. The crest of the barrier is attained after a total displacement of 1.05 Å for each hydrogen atom. Figure 5 shows the profile for this case. The minimum barrier for the C_{2v} pathway is approximately 34.9 kcal/mol above the SiH_2 equilibrium energy. The endothermicity for reaction (4) is 34.27 kcal/mol. The calculated barrier to the (4) backreaction is therefore about 0.63 kcal/mol. Jasinski[17] has determined that the barrier for insertion of D_2 into SiH_2 must be less than 0.9 kcal/mol. Since we expect the insertion barrier onto a bare silicon atom to be similar to that for SiH_2, the result obtained from the global fit is in accord with the available experimental data.[17,18]

As can be seen in Fig. 5, the global surface predicts that there exists a well, 3.41 kcal/mol in depth, in the exit channel for reaction (4). A similar well in the exit channel has been obtained by Viswanathan *et al.*[5(a)] and by Gordon *et al.*[24] for H_2 elimination from silane.

A potential-energy contour map for the C_{2v} dissociation of SiH_2 along a pathway with $\alpha = 21°$ is shown in Fig. 6. The diagonal of this map corresponds to the reaction profile given in Fig. 5. The saddle point is seen at a total displacement of 1.05 Å. The exit channel well occurs at a displacement of about 1.5 Å.

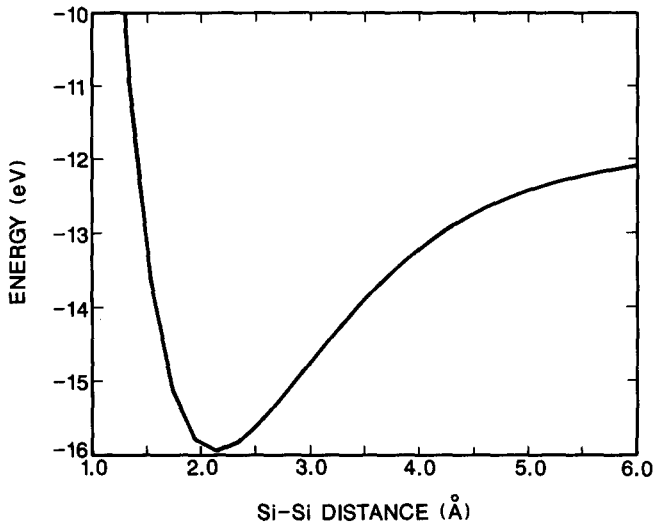

FIG. 4. Dissociation coordinate for Si–Si bond rupture in $H_2Si = SiH_2$. R(Si–H) = 1.4526 Å.

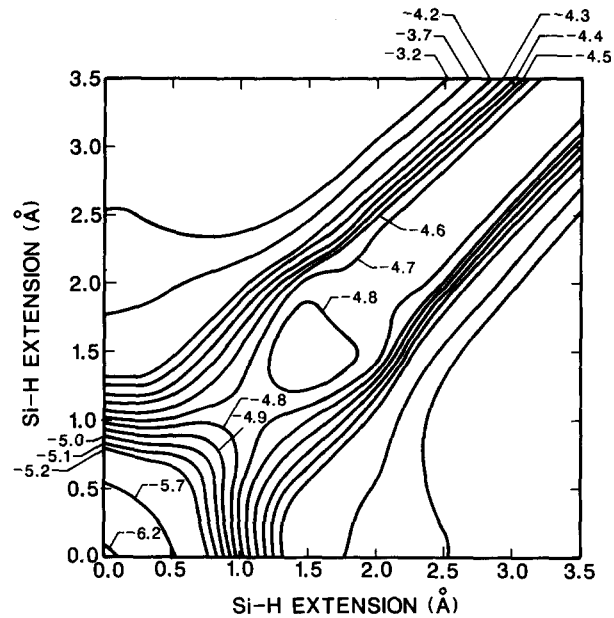

FIG. 6. SiH_2 potential-energy contour map. The axes give the two Si–H bond displacements measured from the equilibrium Si–H separation along the pathway described in the text with $\alpha = 21°$. Contour line energies are given in eV.

The approximate reaction profile and barrier height for the 1,2-H_2 elimination pathway, reaction (3J), has been determined by assuming that the process occurs in the plane containing silicon atom #1 and hydrogen atoms 3 and 5. For a small abstraction distance δ the angles α and β shown in Fig. 7 are varied until the minimum-energy configuration is obtained. This process is repeated until reaction (3J) is essentially complete. Figure 8 shows the reaction profile obtained by the above procedure with the Si–Si bond distance set at 2.314 Å, the equilibrium distance for HSi = SiH, and $\delta = 0.05$ Å. The energy zero is taken to be the energy of the starting configuration which lies 0.2142 eV above that for equilibrium Si_2H_4 due to the increased Si–Si bond distance. The predicted barrier for reaction (3J) along this pathway is 115.3 kcal/mol. The barrier for the backreaction (3J), the four-center insertion of H_2 into HSi = SiH, is calculated to be 30.7 kcal/mol. No *ab initio* calculations of the magnitude of the potential barrier for reaction (3J) have been reported. However, Ho *et al.*[9] have pointed out that such a reaction would require substantial rehybridization of the Si–Si bond and that for the analogous Si_2H_6 reaction they found a large barrier. Consequently, the large barrier predicted by the global surface for reaction (3J) is not unreasonable.

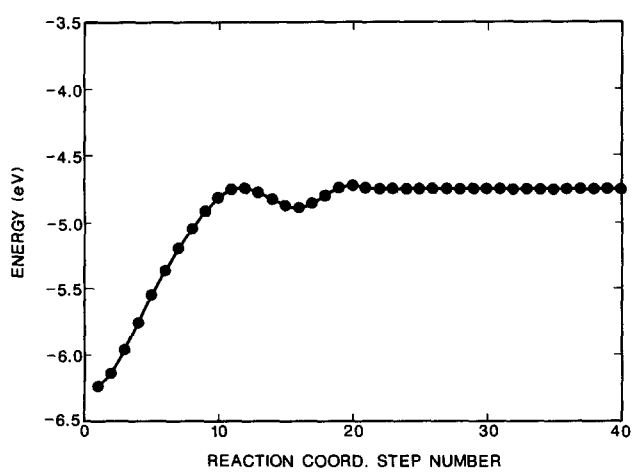

FIG. 5. Reaction profile for molecular hydrogen elimination from SiH_2. Each step corresponds to a C_{2v} symmetric displacement of each Si–H bond by 0.1 Å as described in the text. $\alpha = 21°$.

III. DYNAMICS OF Si_2H_4 FORMATION

In this section, we report the results of trajectory calculations for the cross sections and rates for reaction (3A). Future papers will deal with the decomposition modes and associated rates for Si_2H_4 molecules formed by reaction (3A), microcanonical and thermal rates and associated mechanisms for decomposition of Si_2H_4, and energy transfer mechanisms and rates for this molecule.

A. Computational procedures

Cross sections and rate coefficients for reaction (3A) have been computed using standard quasiclassical trajectory methods.[25] We therefore describe only those procedures that differ in some respect from the standard methods.

Importance sampling[26] with an expected distribution function $P_0(b) = b^{-1}$ is used in the selection of initial im-

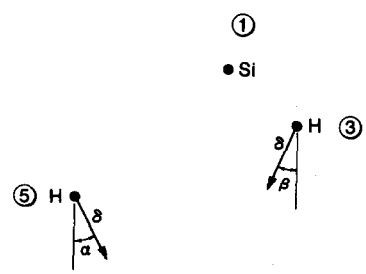

FIG. 7. Plane containing silicon atom #1 and hydrogen atoms 3 and 5. The 1,2-H_2 elimination pathway in this plane is determined by varying angles α and β independently to obtain the minimum-energy structure for a given displacement δ.

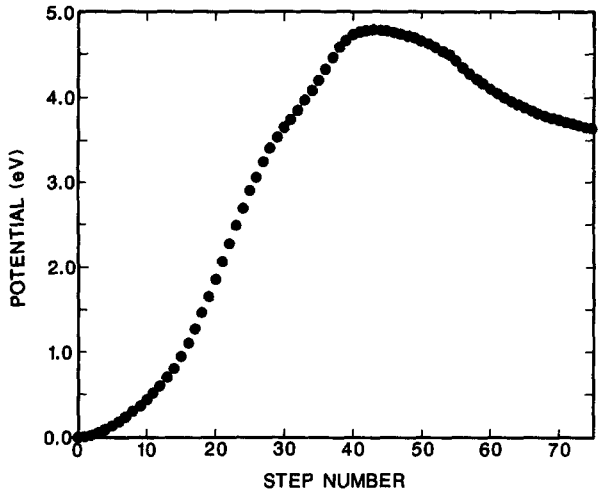

FIG. 8. Reaction profile for 1,2-H_2 elimination from $H_2Si = SiH_2$ along the pathway described in the text and illustrated in Fig. 7. The energy zero is taken to be $H_2Si = SiH_2$ in its equilibrium configuration except for the Si–Si distance which is 2.314 Å. $\delta = 0.05$ Å.

pact parameters. Under these conditions, the impact parameter in the ith trajectory is given by

$$b_i = b_{\max}\xi_i\,, \tag{26}$$

where ξ_i is a random number whose distribution is uniform on the interval [0,1].

With b selected from Eq. (26), the reaction cross section at relative translational energy $E_{\rm Tr}$ for internal rotational and vibrational quantum states denoted by $E_{\rm Rot}$ and v, respectively, is

$$\sigma(E_{\rm Tr},E_{\rm Rot},v) = (2\pi b^2_{\max}/N)\sum_{i=1}^{N_R}\xi_i\,, \tag{27}$$

where the summation runs over the reactive trajectories only and N gives the total number of trajectories examined. A trajectory is considered to be reactive if there exist three inner turning points in the relative Si–Si motion. One sigma limit of statistical uncertainty in these calculations is

$$\Delta\sigma = (2\pi b^2_{\max}/N^{1/2})\left\{\left(\sum_i^{N_R}\xi_i^2\right)\Big/N - \left[\left(\sum_i^{N_R}\xi_i\right)\Big/N\right]^2\right\}^{1/2}. \tag{28}$$

The thermal rate coefficient for reactants in vibrational state v, $k(T,v)$, is given by

$$k(T,v) = [8k_bT/\pi\mu]^{1/2}\sigma(T,v)\,, \tag{29}$$

where k_b is Boltzmann's constant, μ is the system reduced mass and $\sigma(T,v)$ is the cross section for reaction (3A) averaged over the initial translational and rotational energies at temperature T. $\sigma(T,v)$ is computed from Eq. (27) from the results of N trajectories which average over molecular orientations, vibrational phases, impact parameter, and rotational and translational energies as described below:

The three principal moments of inertia I_x, I_y, and I_z for the SiH_2 molecule are 4.46, 2.06, and 2.40 amu Å^2, respectively, where z is taken to be the C_{2v} symmetry axis and x is perpendicular to the SiH_2 plane. We assume the SiH_2 rotational levels are described by those for a symmetric top,

$$E_{jk} = j(j+1)\hbar^2/2I_a + \hbar^2k^2(1/I_x - 1/I_a)/2,$$
$$(j=0,1,2,\ldots),\ (-j\leqslant k\leqslant +j). \tag{30}$$

In Eq. (30), I_a is the average of I_y and I_z. Using this expression, all n rotational energy levels for which $E_{jk} < 30\,k_bT$ are calculated and arranged in increasing order. Each level may then be assigned a single index number, m ($m = 1,2,\ldots,n$). The von Neumann rejection method[27] is now used to select the initial rotational state for each trajectory. That is, we take

$$m = \xi_1 n. \tag{31}$$

The rotational level $E(j_m,k_m)$ is accepted if

$$W(j_m,k_m) > \xi_2\,, \tag{32}$$

where

$$W(j_m,k_m) = Q(j_m,k_m)\Big/\sum_{i=1}^{n}Q(j_i,k_i)\,, \tag{33}$$

with

$$Q(j_m,k_m) = w(2j_m+1)\exp[-E(j_m,k_m)/k_bT],$$
$$w = 2, \quad \text{if } k \text{ is nonzero},$$
$$w = 1, \quad \text{if } k = 0. \tag{34}$$

If Eq. (32) is not satisfied, the procedure is repeated until a rotational state is selected.

The initial momentum components due to rotational motion for each of the atoms in SiH_2 in its equilibrium configuration are

$$\mathbf{P}_i = m_i(\mathbf{w}_i \times \mathbf{r}_i), \tag{35}$$

where $\mathbf{r}$ denotes the position vector of the ith atom of mass m_i in the center-of-mass frame and $\mathbf{w}$ is the angular velocity vector given by

$$E_u = 0.5I_uw_u^2 \quad (u = x,y,z), \tag{36}$$

with

$$E_x = (\hbar^2/2I_x)k_m^2 \tag{37}$$

and

$$E_y = E_z = 0.5[E(j_m,k_m) - E_x]\,. \tag{38}$$

Initial relative velocities are selected from the normalized distribution function[25]

$$F(V) = 2a^2\exp(-aV^2)V^3\,, \tag{39}$$

where $a = \mu/2k_bT$. Initial velocities are again obtained using the von Neumann method[27] with the maximum velocity being taken to be the velocity corresponding to a relative translational energy of $30\,k_bT$.

A harmonic quantization for the three normal SiH_2 vibrational modes has been assumed:

$$E_i = (n_i + 0.5)h\nu_i \quad (i = 1,2,3). \tag{40}$$

At the temperatures of interest in CVD experiments, most of the molecules are in their vibrational ground states. We have therefore carried out most of the calculations with $n_1 = n_2 = n_3 = 0$. However, a few calculations for other vibrational energies have been done to determine the effect of vibrational energy.

Vibrational phase averaging is effected using a combination of the stored structure method[25] and the Porter–Karplus–Sharma[28] procedure. That is, structures are stored over a period of time corresponding to one period of the SiH_2 bending mode T_{vib}. One of these structures is randomly selected for each trajectory and the initial distance between the centers of mass of the two SiH_2 molecules R_s is taken to be

$$R_s = R_s^0 - VT_{vib}\xi/2 . \tag{41}$$

The initial distance R_s^0 has been chosen to be 9 Å for $b < 5$ Å and $b + 5.0$ Å for $b > 5$ Å.

The maximum impact parameter b_{max} has been obtained by examining sets of 20 trajectories at increasing larger values of b_{max} until a value is reached at which the reaction probability goes to zero. A value 0.25 Å larger is then taken for b_{max}. For all sets of calculations with $E_{Tr} > 0.05$ eV, it is found that a range $6.0 < b_{max} < 7.0$ Å is sufficient. When $E_{Tr} = 0.05$ eV, we have used $b_{max} = 9.0$ Å although no trajectory with $b > 6.75$ Å is observed to lead to reaction (3A).

B. Formation cross sections

The cross sections for reaction (3A) for various initial energies in different modes are given in Table V. The cross sections in Table V are arranged into four groups. Group A gives the cross sections when the initial internal energy of both SiH_2 molecules is zero. We see that the cross sections for Si_2H_4 formation increases from 16.6 to 120.2 Å^2 as the relative translational energy is decreased from 1.0 to 0.05 eV. On an attractive surface such as shown in Fig. 3, this is the expected behavior.[23] For energies at or below 0.1034 eV, the formation cross section is becoming almost constant indicating that at low translational energies, the steric hindrance introduced by the presence of the four hydrogen atoms becomes the controlling factor.

In groups B and C, one of the two types of internal energy is initially zero. The translational energy in all calculations in these groups is 0.1034 eV. The internal energies listed in Table V are twice the internal energy present in each SiH_2 molecule. The calculations in group D have the initial translational, vibrational, and rotational energies all nonzero.

A comparison of set II–group A with any of the six sets in groups B and C shows that the presence of initial rotational or vibrational energy decreases the formation cross section by a factor which may be as large as 3. A comparison of the results for sets V and IX shows that the magnitude of the decrease in the cross section increases as the total internal energy present increases. The decrease in the cross sections could be the result of two factors: (1) a transfer of internal energy to relative translational energy which would be expected to result in a decrease of the formation cross section and (2) an increase in the steric hindrance produced by the hydrogen atoms due to rotational motion or to an increase in the vibrational amplitudes as the internal vibrational energy increases. Examination of the initial and final translational energies of trajectories that do not result in the formation of Si_2H_4 shows that there is an appreciable transfer of energy from internal to translational modes. For example, in set V, six out of 28 unreacted trajectories transfer more than 0.17 eV from vibration to translation. When the internal energy is present in the form of zero-point vibrational energy only, such transfer is aphysical since quantum mechanical transfer of this energy is forbidden. If, on the other hand, zero-point energy is omitted, its effect upon the extent of steric hindrance will be lost. Consequently, the treatment of zero-point energy in classical calculations of recombination on attractive surfaces presents a problem.

TABLE V. Si_2H_4 formation cross sections.

Set #	E_{Tr} (eV)	E_{Vib} (eV)[a]	E_{Rot} (eV)[a]	N[b]	Cross section (Å^2)
IA	0.05	0.00	0.00	100	120.2 ± 12.1
IIA	0.1034	0.00	0.00	100	111.6 ± 6.7
IIIA	0.40	0.00	0.00	100	48.8 ± 6.1
IVA	1.00	0.00	0.00	150	16.6 ± 3.5
VB	0.1034	0.6275	0.00	50	51.7 ± 10.4
VIB	0.1034	0.6275 (bend only)	0.00	50	54.9 ± 12.0
VIIB	0.1034	0.6235 (sym. only)	0.00	50	61.2 ± 11.4
VIIIB	0.1034	0.6275 (asym. only)	0.00	50	75.6 ± 11.6
IXB	0.1034	1.1298	0.00	160	35.0 ± 4.1
XC	0.1034	0.00	0.3750	150	33.8 ± 4.4
XID	0.050	0.3772	0.2504	150	30.3 ± 3.8
XIID	0.075	0.3772	0.2504	100	30.8 ± 4.5
XIIID	0.1034	0.3772	0.2504	150	40.3 ± 4.2
XIVD	0.20	0.3772	0.2504	150	34.0 ± 3.7
XVD	0.4	0.3772	0.2504	150	30.1 ± 3.5

[a] The internal energy in each SiH_2 molecule is half the value listed.
[b] Total number of trajectories computed.

A comparison of sets V–VIII give the relative importance of partitioning the initial vibrational energy into the different SiH_2 vibrational modes. In set V, zero-point vibrational energy is present in each mode. In sets VI, VII, and VIII, the same total energy is placed into the bending, symmetric, and asymmetric stretching modes, respectively. It can be seen that the internal energy in the asymmetric stretch is the least effective in decreasing the calculated formation cross sections. An analysis of the unreacted trajectories shows that the energy transfer from vibration to translation is least for this mode. Out of 17 unreacted trajectories, there are two in which energy is transferred from vibration to translation. In these cases, the magnitude of this transfer is less than 0.026 eV. On the other hand, for the bending and symmetric stretch modes, these three numbers are [31, 15, 0.348 eV] and [25, 10, 0.255 eV], respectively.

The magnitude of the increased steric effects produced by the presence of vibrational energy may be estimated by comparing sets VIII and II. Since there is virtually no energy transfer from vibration to translation in set VIII, the difference between the cross section obtained in set II and that for set VIII must be due to the increased steric hindrance. Consequently, such a steric effect is responsible for reducing the cross section from 111.6 to 75.6 $Å^2$. It is therefore an important factor that cannot be ignored.

Comparison of the data for sets XIII or X with V indicates that the presence of initial rotational energy is more effective in reducing the formation cross sections than is a corresponding amount of vibrational energy. This is probably due to the fact that $R \rightarrow T$ transfer is more efficient than $V \rightarrow T$ transfer.

The data for group D sets show that the dependence of the formation cross sections upon relative translational energy is significantly reduced when the internal energy becomes large. A comparison of data sets IV and XV, however, shows that translational energy is more effective than either vibrational or rotational energy in reducing the cross sections.

C. Thermal rate coefficients

Thermal rate coefficients for reaction (3A) may be computed in a straightforward fashion using Eqs. (29)–(41). However, the treatment of the zero-point energy presents a problem. For large systems such as Si_2H_4, the total zero-point energy is many times greater than $k_b T$ and efficient $V \rightarrow T$ transfer creates an aphysical situation that may change the results appreciably for reactions such as (3A). On the other hand, if zero-point energy is omitted in the calculations, then the steric effects due to such energy are lost. As pointed out above, this can also introduce error. Fortunately, the data given in Table V suggest that the problem of aphysical transfer of zero-point energy may not be serious whenever rotational energy is present. The confidence level in the results of classical calculations depends to some extent upon the difference between rate coefficients computed with and without the inclusion of zero-point energy. We therefore report results for both procedures.

Rate coefficients calculated with the inclusion of zero-point energy at temperatures of 300, 800, and 1500 K are given in Table VI. Rate coefficients at 800 K have also been computed without zero-point energy. These results are given in Table VII. The data show that within the statistical accuracy of the calculations, the results are very close. At 800 K, the rate coefficients for reaction (3A) are $(3.62 \pm 0.42) \times 10^{14}$ and $(4.60 \pm 0.54) \times 10^{14}$ cm^3/mol s with and without the inclusion of zero-point energy, respectively. This difference is expected to decrease with increasing temperature. The small difference and the need to include a consideration of steric effects due to vibration suggest that the best procedure is to include zero-point energy in the classical calculations.

The decrease in the average cross section with increasing temperature is a reflection of the fact that cross sections on an attractive potential-energy surface generally decrease with increasing energy.[23] The rate coefficients, on the other hand, exhibit a maximum in the rate coefficient vs temperature curve due to the opposing factors of a collision frequency that increases with $T^{1/2}$ and a cross section that decreases with temperature.

Among the 41 adjustable potential parameters, 36 have been determined by fitting Eq. (1) to the available experimental and theoretical data. However, the values of six parameters, C_1, C_{10}, C_{11}, C_{14}, C_{16}, and C_{21}, have been chosen arbitrarily. It is therefore of interest to determine the sensitivity of the present results to the values of these six parameters. A consideration of the effect of varying the values of the parameters C_{10}, C_{11}, C_{14}, and C_{16} shows that the rate and cross section for reaction (3A) is essentially independent of these parameters. They affect a region of configuration space not sampled in the trajectories undergoing reaction (3A).

TABLE VI. Thermal rate coefficients and average cross sections for reaction (3A) with zero-point energy of vibration in each SiH_2 molecule. Cross sections are given in $Å^2$ and rate coefficients in cm^3/mol s.

Temperature (K)	N[a]	⟨Cross section⟩	$k(T) \times 10^{-14}$
300.0	100	66.2 ± 8.4	2.59 ± 0.33
800.0	150	56.7 ± 6.6	3.62 ± 0.42
1500.0	100	28.7 ± 6.7	2.51 ± 0.59

[a] Total number of trajectories computed.

TABLE VII. Variation in the thermal rate coefficient for reaction (3A) due to change in the initial vibrational energy or potential parameters C_1 and C_{21}. $T = 800$ K. $k(T)$ is given in units of cm^3/mol s.

Vib. energy (eV)[a]	C_1 (1/Å)	C_{21} (1/Å)	N[b]	$k(T) \times 10^{-14}$
0.00	(c)	(c)	100	4.60 ± 0.54
0.1034	(c)	(c)	50	$4\,73 \pm 0.77$
0.6275[d]	(c)	(c)	150	3.62 ± 0.42
0.6275[d]	1.0	(c)	100	2.93 ± 0.47
0.6275[d]	1.0	2.0	100	2.87 ± 0.46

[a] Energy in each SiH_2 molecule is half the value listed.
[b] Total number of trajectories computed.
[c] Value is that given in Table I.
[d] Total zero-point energy.

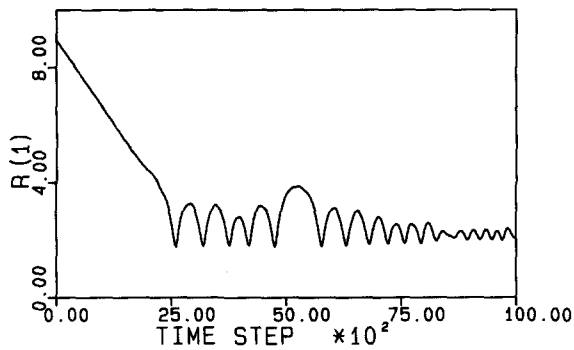

FIG. 9. Variation of the Si–Si distance as a function of time for a typical trajectory. Distances are given in Å; time in units of 2.036×10^{-16} s.

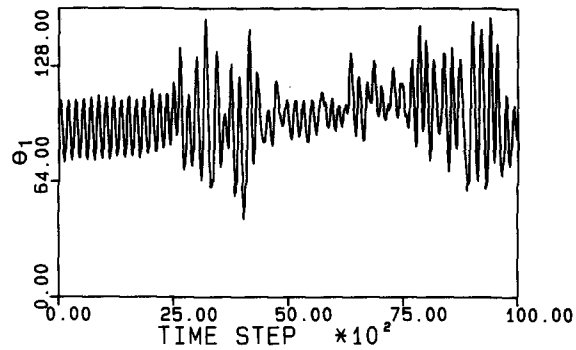

FIG. 11. Variation of one of the H–Si–H bond angles θ_1 with time for the same trajectory illustrated in Fig. 9. Angles are given in degrees. The time units are the same as those in Fig. 9.

Results showing the dependence of the cross section upon C_1 and C_{21} are given in Table VII. As can be seen, an increase in C_1 by a factor of 2 decreases the cross section by a factor of 20% and an increase of C_{21} by a factor of 2 produces less than a 2% decrease in the cross section. Consequently, we do not anticipate that our results will be appreciably affected by any future adjustment of these six parameters.

D. Qualitative aspects of Si_2H_4 formation

An examination of the trajectory details for a collision that results in the formation of Si_2H_4 reveals many qualitative aspects of the reaction and of the energy transfer processes that occur subsequent to formation. Future papers will deal with these questions in more quantitative fashion, but the qualitative examination of such details is itself of interest.

Figures 9–12 show the variation of various interatomic distances and the H–Si–H angles as a function of time for a typical trajectory leading to reaction (3A). For this trajectory, the initial rotational energies of the two SiH_2 molecules are 0.0277 and 0.1120 eV. The translational energy is 0.1128 eV and the impact parameter is 2.94 Å. Both SiH_2 molecules are in their vibrational ground state with zero-point energy included.

Figure 9 gives the distance between the two silicon atoms as a function of time in units of t.u. $= 2.036 \times 10^{-16}$ s. Si–Si bond formation is seen to occur at about 2500 t.u. The reaction exothermicity of 80.45 kcal/mol is primarily partitioned into the Si–Si stretching mode upon formation of Si_2H_4. The resulting large Si–Si stretching amplitude is seen in Fig. 9. Approximately 5000 t.u. after formation of Si_2H_4, this energy is seen to dissipate to other internal modes. Such dissipation therefore occurs on a time scale of about 10^{-12} s. Consequently, it is a relatively slow process compared to intramolecular energy transfer rates that have been computed for other systems where typical transfer times are on the order of $0.2\text{–}0.3 \times 10^{-12}$ s.[29] The decrease in the vibrational period with the decrease in amplitude is a consequence of the anharmonic nature of the Si–Si bond potential.

Figure 10 shows the four Si–H distances as a function of time. The Si–H amplitudes indicate that the SiH_2 vibrational energy is shared equally between the two Si–H bonds. The increase in Si–H amplitude for R_2 and R_3 upon Si_2H_4 formation at 2500 t.u. shows that some of the reaction exothermicity is initially partitioned into Si–H stretching modes. The other two Si–H bonds, however, remain unaffected by Si_2H_4 formation until $t = 7000$ t.u. At this time, energy is transferred from the Si–Si stretch into the Si–H stretching modes associated with silicon atom #2. A careful examination of Fig. 10 also shows the decrease in the equilibrium Si–H bond length that occurs as reaction (3A) takes place.

The time variation of the two H–Si–H angles is shown in Figs. 11 and 12. As reaction (3A) occurs, the H–Si–H equi-

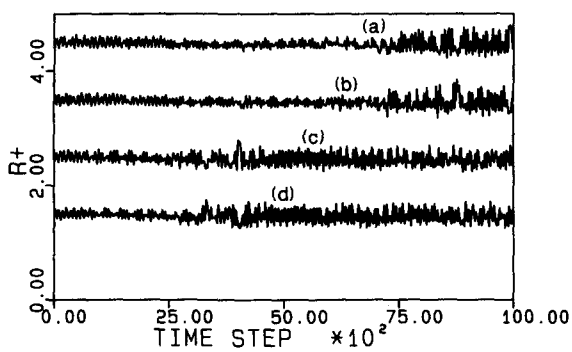

FIG. 10. Variation of the four Si–H distances as a function of time for the same trajectory as illustrated in Fig. 9. Units are the same. (a) $R + = R_5 + 3.0$ Å; (b) $R + = R_4 + 2.0$ Å; (c) $R + = R_3 + 1.0$ Å; (d) $R + = R_2$.

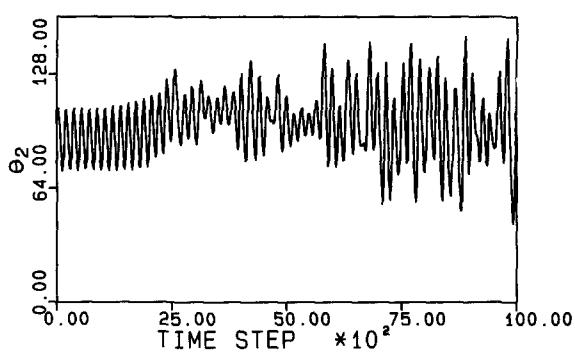

FIG. 12. Variation of the second H–Si–H bond angle θ_2 with time for the same trajectory illustrated in Figs. 9–11. Angles are given in degrees. The time units are the same as those in Figs. 9–11.

librium angle increases from 92.3° to 112.32°. This increase is clearly seen in both figures. As a consequence of this increase, the H–Si–H bending modes will always be excited upon formation of Si_2H_4. The resulting increased bending amplitude is obvious. A comparison of Figs. 10 and 12 shows that energy transfer from the Si–Si stretch to the Si-H stretch is slower than that to the H–Si–H bending mode. This is probably a consequence of the frequency mismatch. The Si–Si and Si–H stretching frequencies are 560 and 2207 (or 2352) cm^{-1}, respectively, whereas the H–Si–H bend is at 960 cm^{-1} on the present potential-energy surface. The near 1:2 resonance between the Si–Si stretch and the H–Si–H bend facilitates energy transfer between these two modes.[30]

IV. SUMMARY

A global potential-energy surface for the Si_2H_4 system has been formulated and fitted to the available experimental and *ab initio* data. The potential surface is the sum of 18 many-body terms. The functional forms of the various terms are chosen so that bending, stretching, and torsional interactions are described by mathematical functions which are motivated by chemical and physical considerations. The surface contains 41 adjustable parameters which are used to fit the surface to calculated geometries, fundamental vibrational frequencies, and energies for $H_2Si=SiH_2$, $H_2Si=SiH$, $H_2Si=Si$, $HSi=Si$, Si_2, H_2, and SiH_2. The surface is also fitted to the $H + H_2$ exchange reaction barrier, to the measured activation energy for insertion of H_2 into SiH_2, and to the estimated barrier for 1,2 elimination of H_2 from $H_2Si=SiH_2$. The fitted surface yields equilibrium geometries for $H_2Si=SiH_2$, $H_2Si=SiH$, $H_2Si=Si$, and SiH_2 in excellent accord with previously reported *ab initio* studies. The error in the bond lengths and angles are usually on the order of 0.03 Å and 0.5°, respectively, or less. The extent of agreement between the predictions of the global surface and previous *ab initio* calculations for the equilibrium structure of $HSi=SiH$ is less. The calculated exothermicities for eight reactions involving these molecules are all in excellent agreement with previous MP4 calculations and experimental data. The average absolute error is 1.90 kcal/mol. Nine of the 41 parameters of the surface have been utilized to fit the calculated fundamental vibration frequencies for $H_2Si=SiH_2$, $H_2Si=SiH$, $H_2Si=Si$, and SiH_2. While an exact fit to the 30 fundamentals is not possible, the degree of accuracy achieved is generally good. The average absolute deviation of the predicted frequencies from the corrected values reported by Ho *et al.*[8,9] is 52.9 cm^{-1}.

The global surface yields a potential barrier height for molecular elimination of H_2 from SiH_2 of 34.27 kcal/mol. The backreaction barrier is 0.63 kcal/mol, which is in good accord with the value suggested by Jasinski's[17] recently reported measurements of the activation energy for the insertion of D_2 into SiH_2. The predicted barrier for the 1,2 elimination of H_2 from $H_2Si=SiH_2$ is 115.3 kcal/mol with a backreaction barrier of 30.7 kcal/mol.

The reaction dynamics for Si_2H_4 formation from $2SiH_2$ molecules have been examined. The formation cross sections are found to decrease with both relative translational energy and internal SiH_2 energy. In the absence of internal SiH_2 energy, the cross section decreases from 120 $Å^2$ at $E_{Tr} = 0.05$ eV to 16.6 $Å^2$ at a translational energy of 1.0 eV. The cross section decreases to 51.72 $Å^2$ for $E_{Tr} = 0.1034$ eV when zero-point vibrational energy is present. The presence of internal SiH_2 angular momentum decreases the formation cross sections even more rapidly. Thermally averaged cross sections vary from 66.3 $Å^2$ at 300 K to 28.7 $Å^2$ at 1500 K. The corresponding rate coefficients exhibit a maximum between 300–1500 K and are on the order of $2–4\times10^{14}$ cm^3/mol s. It is concluded that although there is some aphysical transfer of zero-point energy into relative translational motion, it is still better to include such effects in the classical calculations than to omit them since omission results in the loss of the steric effects produced by the vibrational motion.

Examination of the details of a typical trajectory shows that the reaction exothermicity is primarily partitioned into the Si–Si stretch and H–Si–H bending modes upon formation of Si_2H_4. Energy transfer from the Si–Si stretch to the Si–H stretching modes is a relatively slow process occurring on a time scale of 10^{-12} s. Transfer from the Si–Si stretch to the H–Si–H bending modes is a faster process.

ACKNOWLEDGMENTS

We are pleased to acknowledge financial support from the Air Force Office of Scientific Research under Grant No. AFOSR-86-0043. All calculations in this paper were carried out on a VAX 11/780 and a microVAX II purchased, in part, with funds provided by grants from the Department of Defense University Instrumentation Program, No. AFOSR-85-0115, and the Air Force Office of Scientific Research, No. AFOSR-86-0043. PMA expresses his thanks to Vikram University, Ujjain, India, for granting him leave to pursue this research.

[1](a) M. E. Coltrin, R. J. Kee, and J. A. Miller, J. Electrochem. Soc. **131**, 425 (1984); (b) W. G. Breiland, M. E. Coltrin, and P. Ho, J. Appl. Phys. **59**, 3267 (1986).
[2]P. Ho and W. G. Breiland, Appl. Phys. Lett. **44**, 51 (1984).
[3]D. Martin, D. L. Thompson, and L. M. Raff, J. Chem. Phys. **84**, 4426 (1986).
[4]This value was incorrectly reported in Ref. 3 as -0.028 kcal/mol.
[5](a) R. Viswanathan, D. L. Thompson, and L. M. Raff, J. Chem. Phys. **80**, 4230 (1984); (b) C. G. Newman, H. E. O'Neal, M. A. Ring, F. Leska, and N. Shipley, Int. J. Chem. Kinet. **11**, 1167 (1979).
[6]For a general review of such methods, see D. G. Truhlar, D. Isaacson, and B. C. Garrett, *Generalized Transition State Theory. IV. Theory of Chemical Reaction Dynamics*, edited by M. Baer (Chemical Rubber, Boca Raton, FL, 1985), p. 65.
[7](a) R. Viswanathan, L. M. Raff, and D. L. Thompson, J. Chem. Phys. **80**, 4230 (1984); **81**, 828, 3118 (1984); (b) D. M. Wardlaw and R. A. Marcus, Chem. Phys. Letters, **110**, 230 (1984); (c) D. M. Wardlaw and R. A. Marcus, J. Chem. Phys. **83**, 3462 (1985); (d) D. M. Wardlaw and R. A. Marcus, J. Phys. Chem. **90**, 5383 (1986); (e) J. D. Doll, J. Chem. Phys. **73**, 2760 (1980); **74**, 1074 (1981).
[8]P. Ho, M. E. Coltrin, J. S. Binkley, and C. F. Melius, J. Phys. Chem. **89**, 4647 (1985).
[9]P. Ho, M. E. Coltrin, J. S. Binkley, and C. F. Melius, J. Phys. Chem. **90**, 3399 (1986).
[10](a) J. A. Pople, J. S. Binkley, and R. Seeger, Int. J. Quantum Chem.

Symp. **10**, 1 (1976); (b) R. Krishnan and J. A. Pople, Int. J. Quantum Chem. **14**, 91 (1978); (c) R. Krishnan, M. Frisch, and J. A. Pople, J. Chem. Phys. **72**, 4244 (1980).
[11]M. S. Gordon, T. N. Truong, and E. K. Bonderson, J. Am. Chem. Soc. **108**, 1421 (1986).
[12]R. A. Poirier and J. D. Goddard, Chem. Phys. Lett. **80**, 37 (1981).
[13]K. Krogh-Jespersen, J. Phys. Chem. **86**, 1492 (1982).
[14]S. D. Peyerimhoff and R. J. Buenker, Chem. Phys. **72**, 111 (1982).
[15]J. Berkowitz, J. P. Greene, and H. Cho, J. Chem. Phys. **86**, 1235 (1987).
[16]R. West, M. J. Fink, and J. Michl, Science, **214**, 1344 (1981).
[17]M. J. Fink, M. J. Michalczyk, K. J. Haller, R. West, and J. Michl, J. Chem. Soc. Chem. Commun. **1983**, 1010.
[18]J. M. Jasinski, J. Phys. Chem. **90**, 555(1986).
[19]G. Inoue and M. Suzuki, Chem. Phys. Lett. **122**, 361 (1985).
[20]K. P. Huber and G. Herzberg, *Constants of Diatomic Molecules* (Van Nostrand Reinhold, New York, 1979).
[21](a) L. M. Raff, J. Chem. Phys. **60**, 2220 (1974); (b) R. J. Wolf, D. S. Bhatia, and W. L. Hase, Chem. Phys. Lett. **132**, 493 (1986).
[22]J. S. Binkley, J. Am. Chem. Soc. **106**, 603 (1984).
[23]For example, see (a) L. M. Babcock and D. L. Thompson, J. Chem. Phys. **79**, 4193 (1983); 78, 2394 (1982); (b) W. L. Hase and D. F. Feng, *ibid.* **75**, 738 (1981); (c) K. N. Swamy and W. L. Hase, *ibid.* **77**, 3011 (1982); (d) J. Am. Chem. Soc. **106**, 4071 (1984); (e) S. L. Mondro, S. V. Linde, and W. L. Hase, J. Chem. Phys. **84**, 3783 (1986).
[24]M. S. Gordon, D. R. Gano, J. S. Binkley, and M. J. Frisch, J. Am. Chem. Soc. **108**, 2191 (1986).
[25]L. M. Raff and D. L. Thompson, *Classical Trajectory Approach to Reactive Scattering. III. Theory of Chemical Reaction Dynamics*, edited by M. Baer (Chemical Rubber, Boca Raton, FL, 1985).
[26]M. B. Faist, J. T. Muckerman, and F. E. Schubert, J. Chem. Phys. **69**, 4087 (1978).
[27]J. von Neumann, J. Res. Nat. Bus. Stand. Appl. Math. Ser. **3**, 36 (1951).
[28]M. Karplus, R. N. Porter, and R. D. Sharma, J. Chem. Phys. **43**, 3259 (1965).
[29]K. L. Bintz, D. L. Thompson, and J. W. Brady, J. Chem. Phys. **85**, 1848 (1986).
[30]See, for example, (a) S. Shi and W. H. Miller, Theor. Chim. Acta **68**, 1 (1985); (b) C. J. Cerjan, S. Shi, and W. H. Miller, J. Phys. Chem. **86**, 2244 (1982); (c) E. L. Sibert, J. T. Hynes, and W. P. Reinhardt, J. Chem. Phys. **81**, 1135 (1982); (d) E. L. Sibert, W. P. Reinhardt, and J. T. Hynes, *ibid.* **81**, 1115 (1984); (e) E. L. Sibert, W. P. Reinhardt, and J. T. Hynes, Chem. Phys. Lett. **92**, 455 (1982).